Noncovalent Shiga-like Toxin Assemblies: Characterization by Means of Mass Spectrometry and Tandem Mass Spectrometry†

Jonathan P. Williams,*,‡ Brian N. Green,§ Daniel C. Smith,‡ Keith R. Jennings,‡ Katherine A. H. Moore,‡ Susan E. Slade,‡ Lynne M. Roberts,‡ and James H. Scrivens‡

Department of Biological Sciences, University of Warwick, Gibbet Hill Road, Coventry CV4 7AL, U.K., and Waters MS Technologies Centre, Micromass UK Ltd., Atlas Park, Simonsway, Manchester M22 5PP, U.K.

Received February 28, 2005; Revised Manuscript Received April 21, 2005

ABSTRACT: Shiga-like toxin 1 (SLTx), produced by enterohemorrhagic strains of *Escherichia coli* (EHEC), belongs to a family of structurally and functionally related AB_5 protein toxins that are associated with human disease. EHEC infection often gives rise to hemolytic colitis, while toxin-induced kidney damage is one of the major causes of hemolytic uremic syndrome (HUS) and acute renal failure in children. As such, an understanding and analysis of the noncovalent interactions that maintain the quaternary structure of this toxin are fundamentally important since such interactions have significant biochemical and medical implications. This paper reports on the analysis of the noncovalent homopentameric complex of Shiga-like toxin B chain (SLTx-B_5) using electrospray ionization (ESI) triple-quadrupole (QqQ) mass spectrometry (MS) and tandem mass spectrometry (MS/MS) and the analysis of the noncovalent hexameric holotoxin (SLTx-AB_5) using ESI time-of-flight (TOF) MS. The triple-quadrupole analysis revealed highly charged monomer ions dissociate from the multiprotein complex to form dimer, trimer, and tetramer product ions, which were also seen to further dissociate. The ESI-TOFMS analysis of SLTx-AB_5 revealed the complex remained intact and was observed in the gas phase over a range of pHs. Theses findings demonstrate that the gas-phase structure observed for both the holotoxin and the isoloated B chains correlates well with the structures reported to exist in the solution phase for these proteins. Such analysis provides a rapid screening technique for assessing the noncovalent structure of this family of proteins and other structurally related toxins.

Shiga-like toxin 1 (SLTx),[1] produced by enterohemorrhagic strains of *Escherichia coli* (EHEC) (*1*), belongs to a family of structurally and functionally related AB_5 protein toxins that are associated with human disease (*2*). EHEC infection often gives rise to hemorrhagic colitis (*2*, *3*), while toxin-induced kidney damage is one of the major causes of hemolytic uremic syndrome (HUS) and acute renal failure in children (*4*). The structures of both the SLTx holotoxin and the SLTx-B subunit have been determined by X-ray crystallography and NMR studies (*5*−*7*). The A subunit (∼32 kDa) is positioned on one face of the noncovalently associated B chain homopentamer (∼7.8 kDa/subunit), with the C-terminus of the A chain anchored noncovalently in its central pore (Figure 1A). The SLTx A subunit is an *N*-glycosidase that specifically removes a conserved adenine residue from the EF-2 binding site of 28S rRNA (*8*), thereby inhibiting cellular protein synthesis and promoting cell death (*9*). SLTx specifically binds, via its B pentamer, to the glycosphingolipid, globotriaosylceramide (Gb3) (*10*−*12*), on the surface of certain types of mammalian cells. Following binding, the toxin−lipid complex is rapidly internalized by endocytosis, where the A subunit is proteolytically nicked between an intrachain disulfide bond, generating a covalently linked A1 (∼29 kDa) and A2 (∼3 kDa) fragment (*13*, *14*). The complex is then routed in a retrograde manner to the endoplasmic reticulum (ER) via the trans-Golgi network (*15*−*17*). Within the ER, it is thought that the A1 fragment is reductively separated from the A2−B_5 complex and subsequently translocated across the membrane into the cytosol. The specificity of binding and efficient intracellular routing along this productive pathway, combined with a high rate of enzymatic turnover, make SLTx an extremely potent toxin to susceptible cells. In addition to the well-documented cytotoxic nature of SLTx, interactions between the SLTx holotoxin or its pentamer and specific target cells can also promote signaling events leading to immunomodulatory functions in certain cell types and apoptosis in others (*18*). Recently, SLTx has been utilized for different therapeutic applications ranging from the delivery of antigenic peptides (*19*−*22*) and immunomodulation of antigen-presenting cells (*23*) to the diagnosis of certain tumors (*24*). A key element in the diverse activities of this toxin is the initial oligomer-

† Work in this study was supported by Wellcome Trust Program Grant 063058/Z/00/Z to L.M.R.

* To whom correspondence should be addressed: Department of Biological Sciences, University of Warwick, Gibbet Hill Road, Coventry CV4 7AL, U.K. Fax: 02476523701. Telephone: 02476522157. E-mail: j.p.williams@warwick.ac.uk.

‡ University of Warwick.

§ Micromass UK Ltd.

[1] Abbreviations: SLTx, Shiga-like toxin 1; SLTx-B_5, homopentamer of the Shiga-like toxin; SLTx-AB_5, hexameric holotoxin of the Shiga-like toxin; ESI, electrospray ionization; MS, mass spectrometry; MS/MS, tandem mass spectrometry; TOFMS, time-of-flight mass spectrometry; CID, collision-induced dissociation; SDS−PAGE, sodium dodecyl sulfate−polyacrylamide gel electrophoresis.

10.1021/bi0503706 CCC: $30.25
Published on Web 05/19/2005

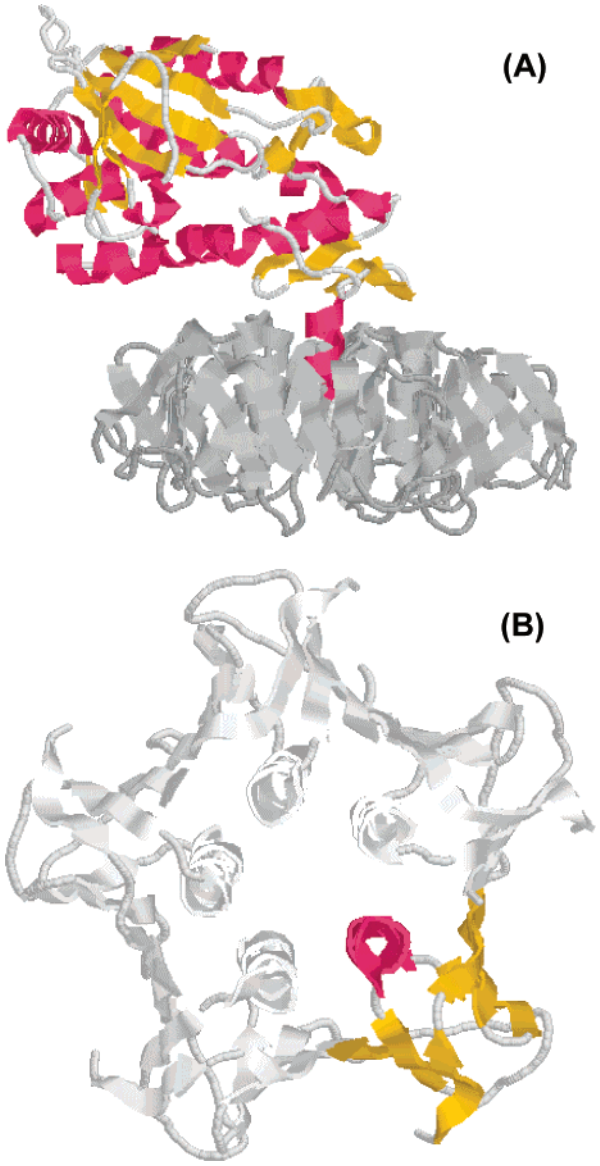

FIGURE 1: Crystal structure of the SLT B chain pentamer and Shiga-like toxin (SLT). (A) SLT holotoxin viewed sideways with the surface of the B pentamer that contains the membrane binding sites facing downward. The catalytic A chain is colored to show secondary structure. The A2 fragment can be seen to insert into the core of the B pentamer. (B) SLT B chain pentamer shown from the top, with a single monomer colored to indicate secondary structure (α helix in red and β sheet in yellow).

ization of Gb3 receptors upon binding the B chain pentamer. This is believed to promote recruitment into lipid rafts for intracellular trafficking (*25*−*27*) and to establish signaling cascades (*28*−*30*). As such, an understanding and analysis of the noncovalent interactions that maintain the quaternary structure of this toxin is fundamentally important since such interactions have significant biochemical and medical implications.

Electrospray ionization (ESI) (*31*) is a powerful technique that aids the study of biological noncovalent assemblies. ESI permits the assemblies to be transferred from the liquid phase to the gas phase intact, allowing detection by mass spectrometry (MS). To study intact noncovalent assemblies by means of ESI-MS, the internal energy of the ions formed by the electrospray process must be kept to a minimum to avoid dissociation. Collisional stabilization is accomplished by increasing the backing pressure between the source and ion guide interface region of the mass spectrometer (*32*−*34*). Very large noncovalent assemblies have been observed in this way, including the intact MS2 virus capsid at ~2.5 MDa (*35*), rice yellow mottle virus at ~6.5 MDa, and tobacco mosaic virus at ~40.5 MDa (*36*), but there have been fewer reports of the characterization of noncovalent assemblies by means of tandem mass spectrometry (MS/MS). Early studies were conducted on the tetrameric assemblies of human hemoglobin (*37*) which was found to dissociate with the formation of monomeric and trimeric product ions. More recently, gas-phase dissociations for the tetrameric complex transthyretin [~55.5 kDa (*38*)] and the chaperone GroEL [~800 kDa (*39*)] have been reported.

In this study, ESI-MS and ESI-MS/MS have been used to examine the noncovalent interactions that exist between the subunits of the complete SLTx holotoxin or the pentameric B subunit. The ability to rapidly identify and characterize such interactions will be very important for future research into this class of pathogenic protein. The first objective of this investigation was to examine the ions produced from the complete hexameric noncovalent holotoxin complex (SLTx-AB_5). Our results clearly show that the intact complex was observed in the gas phase of a time-of-flight mass spectrometer over a range of pHs, including one representing physiological conditions. Furthermore, we report the dissociation of the noncovalent homopentameric binding subunit of the toxin (SLTx-B_5), by means of in-source collision-induced dissociation (CID) and CID in a collision cell of a triple-quadrupole mass spectrometer allowing us to probe the gas-phase dissociation pathways. Pseudo-MS/MS/MS experiments were also performed with the homopentamer by subjecting the pentamer ions to CID within the source region of the mass spectrometer prior to the precursor fragment ion being selected for CID in a collision cell, thereby allowing their dissociation pathways to be established.

MATERIALS AND METHODS

Expression and Purification of Recombinant SLTx and SLTx B Chain. Recombinant SLTx holotoxin or SLTx-B was expressed in a 1 L culture of *E. coli* JM105 cells harboring pUC19 containing either the SLTx bicistronic operon or the SLTx-B gene, respectively, during a 4 h induction with 1 mM isopropyl 1-thio-β-D-galactoside. Cells were harvested, resuspended in 20% (w/v) sucrose, 300 mM Tris-HCl (pH 8.0), 1 mM EDTA, and 0.5 mM $MgCl_2$, repelleted, and resuspended in 10 mL of ice-cold 1 mM Tris-HCl (pH 7.5) to osmotically lyse the cells' periplasm and release assembled SLTx or SLTx-B oligomers. The resulting high-speed supernatant was filter-sterilized and applied to a 1 mL synthetic globotriose−Sepharose affinity chromatography column equilibrated in PBS. SLTx or SLTx-B was subsequently eluted with 6 M guanidine hydrochloride and immediately dialyzed against PBS overnight, and selected samples were quantified and analyzed by reducing SDS−PAGE. Purified toxin samples were extensively dialyzed against 10 mM ammonium acetate (Sigma) at pH 7.0, desalted using PD-10 gel filtration columns, and concentrated to a final protein concentration of 7 μM for SLTx holotoxin and 236 μM for SLTx-B in a Centricon 10 apparatus (Amicon).

Mass Spectrometry. Experiments were performed in a triple-quadrupole mass spectrometer (Quattro Ultima, Waters MS Technologies, Manchester, U.K.) and a single time-of-flight mass spectrometer (LCT, Waters MS Technologies). Both instruments were equipped with the standard Z-spray electrospray ion source and operated at a source and desolvation temperature of 110 °C. Sample solutions were introduced into the source region of the instruments by conventional electrospray, operated in the positive mode of ionization, with a capillary voltage of 3 kV, and were optimized for the transmission of noncovalent complexes. In each instrument, noncovalent complexes were observed by increasing the pressure between the source and high-vacuum region. In-source CID (pseudo-MS^2) mass spectra were observed by increasing the declustering potential (cone voltage) on the time-of-flight instrument. In the triple-quadrupole instrument, in-source CID mass spectra were observed by increasing the potential difference between the ion guides, RF lens 1 and RF lens 2. Tandem mass spectrometry (MS/MS or MS^2) on this instrument was carried out using argon as the collision gas at a pressure of 2.5×10^{-3} mbar within the RF-only hexapole collision cell. Pseudo-MS/MS/MS (pseudo-MS^3) experiments were performed similarly, the precursor fragment ion being selected prior to entering the collision cell.

For the different charge states analyzed in the triple-quadrupole instrument operated in the in-source CID/precursor ion MS/MS mode, the instrumental settings were further optimized by careful adjustment of the RF lens 1 voltage, within the range of 40−70 V which produced collision energies within the range of 5−40 eV, thereby increasing the level of fragmentation over the mass range of interest. Data acquisition and processing were carried out using MassLynx (version 3.5). Transform, or alternatively, Maximum Entropy-based software (*40*) was used to find the masses of the subunits and hence the charges on each multiply charged ion. All spectra that are shown were subjected to minimal smoothing. The upper *m*/*z* range of the triple-quadrupole instrument is 4000. Ions of the type B_x^{y+} could be observed only if $y \geq 2x$, since the monomer has a mass of nearly 7700.

The complex formed by the homopentameric binding subunit of the Shiga-like toxin (SLTx-B_5) and the hexameric holotoxin (SLTx-AB_5) were studied by direct infusion at a flow rate of 4 μL/min, using a Harvard Apparatus (South Natick, MA) model 22 syringe pump, at a concentration of 10 pmol/μL in 10 mM aqueous ammonium acetate at pH 3.0−7.5, adjusted by addition of dilute ammonia or formic acid solution. As discussed in a subsequent section, the AB_5 hexameric holotoxin was desalted manually by undergoing shaking for 1 min with previously washed mixed bed ion exchange beads (Bio-Rad, AG 501-X8, catalog no. 143-7424).

RESULTS AND DISCUSSION

Triple-Quadrupole MS for the AB_5 Holotoxin. Initially, the recombinantly expressed and purified preparation of SLTx holotoxin (2 pmol/μL) was analyzed denatured in a solution of acetonitrile/H_2O with 0.2% formic acid. While the analysis confirmed the homogeneity of the B protein component, the A protein was heterogeneous and consisted of four components (Figure 2A). Maximum Entropy provided the molecular mass of 7688.5 Da for the SLTx B subunit (sequence mass of 7688.7 Da) and masses of 31 531.6, 31 602.4, 31 734.1, and 31 890.3 Da for the heterogeneous SLTx A protein. These results are the mean of four separate measurements. A typical Maximum Entropy deconvoluted spectrum obtained for one of the measurements clearly identifies four different major components for the A protein (Figure 2B).

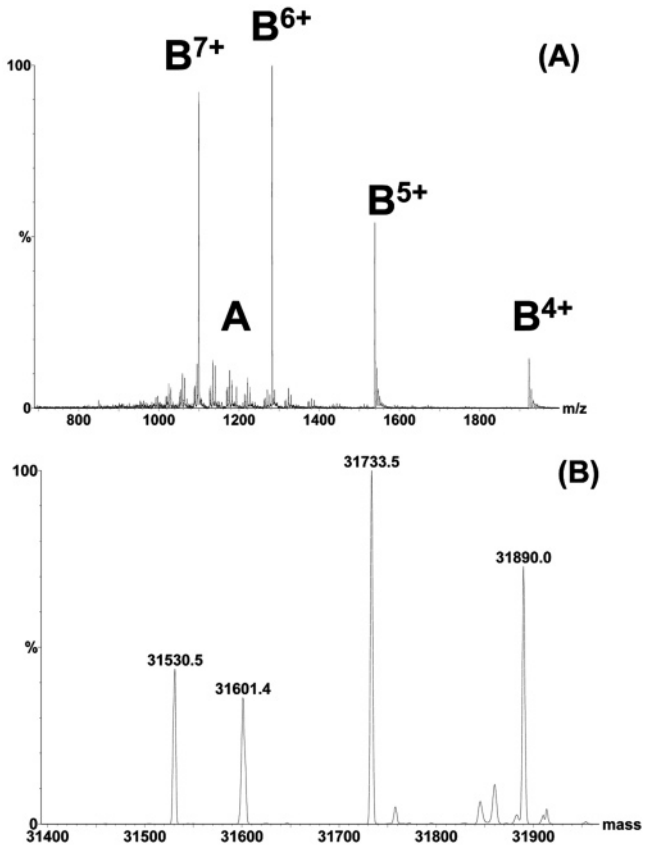

FIGURE 2: ESI triple-quadrupole mass spectrum of the denatured Shiga-like holotoxin at a concentration of 2 pmol/μL in an acetonitrile/H_2O mixture with 0.2% formic acid (A). Maximum Entropy deconvoluted spectrum expanded in the region from *m*/*z* 31 400 to 31 950 highlighting the heterogeneity of the A unit (B).

The heterogeneity observed within the A chain of the protein most likely reflects selective protease trimming during bacterial expression. Periplasmic expression offers numerous advantages for the production of toxic proteins such as SLTx. However, expression can be limited by degradation within the periplasmic space. Indeed, the bacterial periplasm contains many endo- and exo-proteases with more than 20 being identified in *E. coli*, of which approximately 50% are localized in the periplasm (*41*, *42*). It is conceivable, therefore, that during SLTx expression within the periplasm, the A chain is partially trimmed, at the amino terminus, the carboxy terminus, or both, thus generating smaller polypeptide chains.

Time-of-Flight MS for the AB_5 Holotoxin. Previously, nanoelectrospray was performed on a 10 pmol/μL aqueous solution of the holotoxin, and at pH 3.5, AB_5 ions were observed (*43*); however, it was reported that at neutral pH only a weak ion signal corresponding to the polyprotonated B_5 pentamer was observed. It was assumed that the AB_5 ions were being generated by the nanoelectrospray process at neutral pH but at mass-to-charge (*m*/*z*) ratios that exceeded

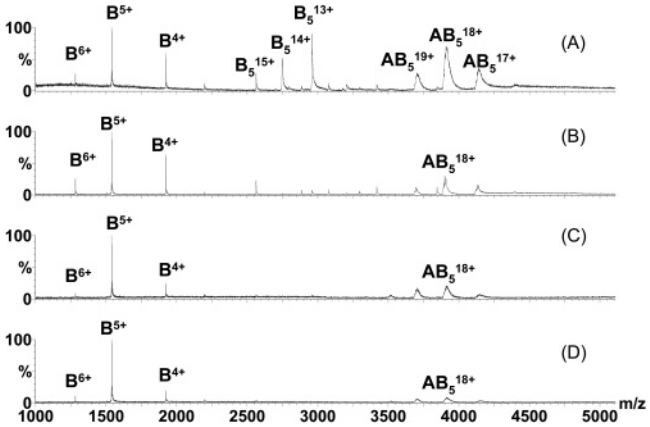

FIGURE 3: ESI-TOF mass spectra obtained for the AB_5 Shiga-like holotoxin buffered with ammonium acetate at various pHs. Shown is the noncovalent assembly at pH 7.0 and CV = 50 V (A), pH 6.6 and CV = 70 V (B), pH 3.5 and CV = 40 V (C), and pH 3.0 and CV = 40 V (D).

the capability of the FTICR mass spectrometer (*m*/*z* 5000). To test this assumption, a study of the toxin was carried out in the time-of-flight instrument at different pH values (Figure 3). Our data confirm those of a previous investigation (*43*) showing that the AB_5 holotoxin remains intact during the electrospray process. However, in contrast to the results of the previous study (*43*), the mass spectra obtained for the holotoxin show a strong signal for both the B_5 pentamer and the AB_5 holotoxin at pH ~7 (Figure 3). Our data clearly show that within the pH range of 3−7, the same three protonated holotoxin AB_5 ions are formed (17+, 18+, and 19+) and no holotoxin ions were observed beyond *m*/*z* 5000. At pH ~3.0−3.5, only monomer B ions and holotoxin AB_5 ions are observed, but as the pH is increased to ~6.6−7.0, these ions are observed together with the pentamer B_5 ions. The relative abundance of the AB_5 holotoxin ions decreases as the pH is reduced from 6.6. In the pH range of 3.0−3.5, only partial decomposition of the AB_5 holotoxin was observed compared to that at neutral pH, possibly suggesting the AB_5 holotoxin is more stable than the B_5 pentamer at lower pH. The pH sensitivity of the B_5 pentamer is consistent with a previous report showing that at acidic pH (≤4.5) the secondary structure of the B_5 pentamer, as monitored by circular dichroism, is significantly altered (*44*). The increased stability of the AB_5 holotoxin compared to the B_5 pentamer at a lowered pH may arise from interactions occurring between SLTx A2 and the helices that line the pore in the B_5 pentamer. Structural analysis of the holotoxin shows that the SLTx A subunit is positioned asymmetrically within the B_5 pentamer, simultaneously associating with three of the five B subunits (*6*). This noncovalent interaction is thought to involve both a network of hydrogen bonds and van der Waals forces leading to a strong association of the A and B_5 subunits (*45*).

Since heterogeneity of the SLTx A chain had been observed (Figure 2), we further examined the SLTx holotoxin by TOFMS under conditions that maintained the noncovalently associated holotoxin intact in the gas phase. The mass spectrum of the intact holotoxin generated peaks showing detection of more than one component, which were partially resolved from each other (data not shown) when the cone voltage of the instrument was increased beyond 70 V. Furthermore, as previously reported (*46*), as the cone

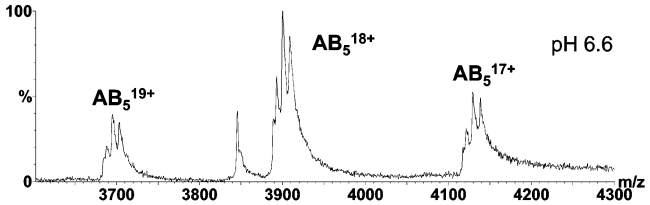

FIGURE 4: ESI-TOF mass spectra obtained for the AB_5 Shiga-like holotoxin buffered with ammonium acetate at pH 6.6. Shown is the noncovalent assembly mass spectrum expanded in the region from *m*/*z* 3600 to 4300 after the desalting procedure.

voltage in the TOF instrument is increased, the peak widths of the ions decrease, suggesting the loss of low-molecular mass noncovalent adducts from species formed in solution. Even though the sample had been desalted, additional desalting using mixed bed ion exchange beads improved the peak width and provided better resolution of the various components. The spectrum obtained clearly shows heterogeneity within the AB_5 ions detected with a cone voltage of 70 V at pH ~6.6 (Figure 4). Transformation of the spectrum in the region of *m*/*z* 3500−4500, which corresponds to the ions observed for the holotoxin, gave suggested molecular masses of 69 981 Da (calcd, 69 974.9 Da), 70 051 Da (calcd, 70 045.7 Da), 70 184 Da (calcd, 70 177.4 Da), and 70 337 Da (calcd, 70 333.6 Da), for the heterogeneous AB_5 holotoxin, which shows good agreement with that expected for the hexameric complex. These molecular masses are in good agreement with those calculated previously (Figure 2).

Here we have demonstrated that the complete noncovalent complex of SLTx holotoxin, in contrast to previous studies (*43*), can be detected by ESI-TOF mass spectrometry over a range of pHs. As far as we know, this is the first time the holotoxin complex has been observed intact at physiological pH. The increased sensitivity afforded by time-of-flight mass analyzers for observing such complexes intact in the gas phase has been demonstrated. The high degree of sensitivity also allowed for the accurate detection of differentially trimmed species of the A chain within the holotoxin preparation. This level of structural information will have obvious benefits for research into the intracellular transport and processing pathways of SLTx during cellular intoxication. However, as the TOF instrument is not capable of tandem mass spectrometry experiments, further examination was performed solely on the B chain pentamer.

Triple-Quadrupole MS for the B_5 Homopentamer. The SLTx pentamer B_5 consists of five identical subunits that arrange into a pentameric ring structure (Figure 1B). Each subunit has a molecular mass of 7.7 kDa and is composed of 69 amino acids that form two three-stranded antiparallel β sheets and an α helix (*5*, *47*). Analysis of the SLTx B chain preparation (2 pmol/μL) in an acetonitrile/H_2O mixture with 0.2% formic acid confirmed the homogeneity of the protein (Figure 5, inset). Maximum Entropy suggested a molecular mass of 7688.5 Da for the B subunit which is in good agreement with the predicted mass. The mass spectrum obtained for the noncovalent complex of SLTx-B_5 buffered with ammonium acetate at pH ~6.6 clearly shows that the isolated B pentamer remains intact during the electrospray process (Figure 5). The mass spectrum was obtained with a low voltage (40 V) applied to RF lens 1. The base peak in the mass spectrum corresponds to B_5^{13+}. The dominant signal corresponds to the intact homopentamer, labeled B_5. The

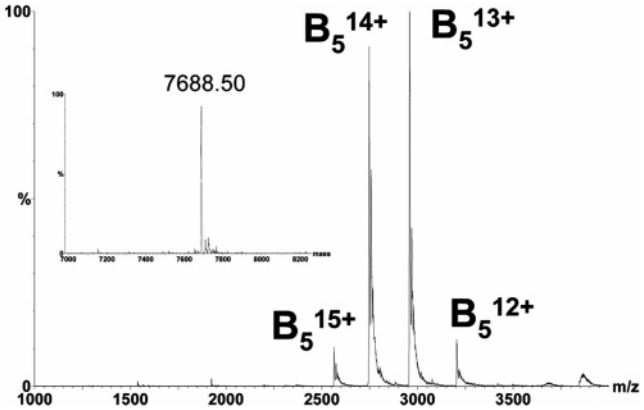

FIGURE 5: ESI triple-quadrupole mass spectrum of the noncovalent complex of SLT-B_5 and an inset showing the Maximum Entropy deconvoluted spectrum of the monomer subunit.

observed charge states extend from 15+ to 12+. The mass spectrum demonstrates that the homopentamer B_5, the dominant form of the B subunit protein in solution, remains intact during the electrospray process. Mass spectra obtained previously (*43*), and during this investigation for the noncovalent complex of the B_5 homopentamer, demonstrate that under the specified conditions the pentamer is stable and can be transferred from the liquid phase to the gas phase intact.

Next, in-source CID of the B_5 pentamer was performed by increasing the potential difference between the ion guides, RF lenses 1 and 2 (Figure 6). As the voltage applied to RF lens 1 is increased from 50 V (Figure 5, top spectrum) to 60 V (Figure 6, bottom spectrum), the homopentamer dissociates to the monomer ($B^{3+}-B^{6+}$), and possibly low-abundance dimer (B_2^{7+}), trimer ($B_3^{6+}-B_3^{8+}$), and tetramer (B_4^{9+} and B_4^{10+}) ions. At an applied RF lens 1 voltage of 60 V, the base peak in the mass spectrum shifts to the monomer B^{5+} ion.

Our results are consistent with a previous investigation (*43*) which suggested that the SLTx B pentamer dissociates almost entirely via the loss of a single B subunit. Our data correlate well with experimental data obtained with the toxin in the solution phase. Indeed, electrophoretic analysis of the protein coupled to structural and thermodynamic studies (*48*, *49*) indicates that the B chain exists predominantly in a pentameric state in aqueous solution, which when disrupted collapses to a monomeric species with little or no intermediate observed structure (*49*).

Triple-Quadrupole MS/MS of the B_5 Homopentamer. Tandem mass spectrometry (MS/MS) was used to investigate the dissociation pathways of the SLTx B_5^{13+}, B_5^{14+}, B_4^{9+}, B_3^{6+}, and B_3^{7+} ions. The two dominant ions in the mass spectrum of the homopentamer correspond to B_5^{13+} and B_5^{14+}. They were selected as precursor ions to undergo CID in the collision cell of the instrument, the collision energy being varied to obtain intense fragment ions (product ions). The MS/MS spectrum for B_5^{14+} obtained at collision energies of 15 V (Figure 7A) and 25 V (Figure 7B) illustrate the increased abundance of product ions as the collision energy is increased. Similar MS/MS spectra were obtained for the B_5^{13+} ion at collision energies of 15 V (Figure 7C) and 18 V (Figure 7D). The multiply protonated pentamer species B_5^{14+} and B_5^{13+} selected for CID dissociate almost entirely via the loss of one subunit (Figure 7E) to form monomer, trimer, and tetramer ions, but no peaks which could be unequivocally assigned to dimer ions were observed. These ions might still have been formed; however, the B_2^{2+}, B_2^{4+}, and B_2^{6+} ions cannot be distinguished from the B^+, B^{2+}, and B^{3+} ions, B_3^{3+}, B_3^{6+}, and B_3^{9+} ions, and B_4^{4+}, B_4^{8+}, and B_4^{12+} ions, respectively, to which some of the peaks have been assigned. However, not all of the ions that are predicted to form (Figure 7E) were detected. This was either due to them being present in very low abundance or due to the *m*/*z* ratio of the ion being beyond the upper *m*/*z* range of the instrument, 4000, as discussed above. These results are consistent with those observed previously when the B_5 complex was thermally decomposed by blackbody infrared radiative dissociation (BIRD) within the cell of a Fourier transform ion cyclotron resonance (FT-ICR) mass spectrometer (*50*). Furthermore, the MS/MS data obtained in our study correlate well with, and extend, our in-source CID analysis (Figure 6), again indicating that SLTx B pentamer dissociation occurs via the sequential loss of a single B subunit.

Triple-Quadrupole Pseudo-MS/MS/MS for B_4 and B_3 Ions. Previous results indicated that B_4 ions resulting from the loss of a single subunit were resistant to further dissociation over the temperature range that was studied (*50*). The B_4^{9+}, B_3^{6+}, and B_3^{7+} ions, formed from in-source CID, were therefore subjected to CID in the collision cell in an effort to investigate their fragmentation under these conditions. The mass spectrum obtained in the absence of the collision gas (Figure 8A) shows that the B_4^{9+} ion does not undergo further dissociation between ion guide RF lens 2 and the detector prior to CID within the collision cell. With a collision gas in the cell and ion collision energies of 5 and 15 eV, two sets of products were formed (Figure 8A). These products represent monomer ion B^{3+} together with trimer ion B_3^{6+} and the momomer B^{4+} ion, which is presumably accompanied by the B_3^{5+} trimer ion which is not observed as its *m*/*z* ratio of 4614 is outside the range of the instrument (Figure 8B). At the higher collision energy, the precursor ion is no longer observed, suggesting complete dissociation of the B_4^{9+} ion.

The B_3^{6+} ion was shown not to undergo further dissociation when passed through the collision cell in the absence of a collision gas (Figure 8C), but when a collision gas was introduced, the main product observed was the B^{3+} ion with a small amount of the B^{4+} ion being formed at higher collision energies (Figure 8C). The other products which are expected to accompany these two products are the B_2^{3+} and B_2^{2+} ions, both of which lie outside the *m*/*z* range of the instrument and are therefore not observed as indicated in the dissociation scheme (Figure 8D).

The CID mass spectrum of trimer ion B_3^{7+} obtained at two collision energies indicates that this ion can further dissociate (Figure 8E). The major products that are observed are the B^{2+} and B^{3+} ions, together with the B_2^{5+} ion observed at low abundance at the higher collision energy and the B_2^{4+} ion which presumably contributes to the peak labeled B^{2+}, shown in the dissociation scheme (Figure 8F).

Previous results (*50*) obtained via BIRD in an FTICR mass spectrometer concluded that the B_4 ions were resistant to further dissociation over the temperature range that was studied. Our data obtained by pseudo-MS/MS/MS experiments on the B_4^{9+}, B_3^{6+}, and B_3^{7+} ions show that these ions do undergo further dissociation, forming product ions which suggest the loss of a further B subunit. This sequential loss

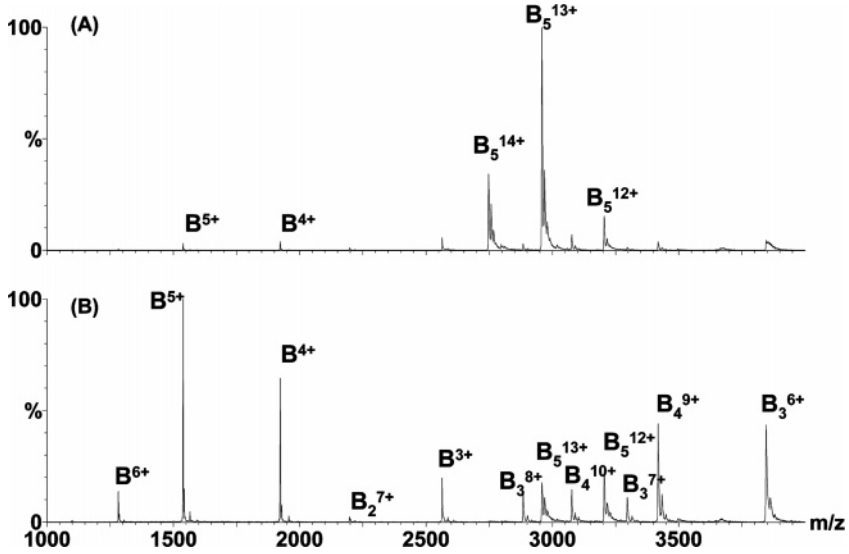

FIGURE 6: ESI triple-quadrupole in-source CID mass spectra of the noncovalent complex of SLT-B_5. Shown is the dissociation obtained at voltages of 50 (A) and 60 V (B).

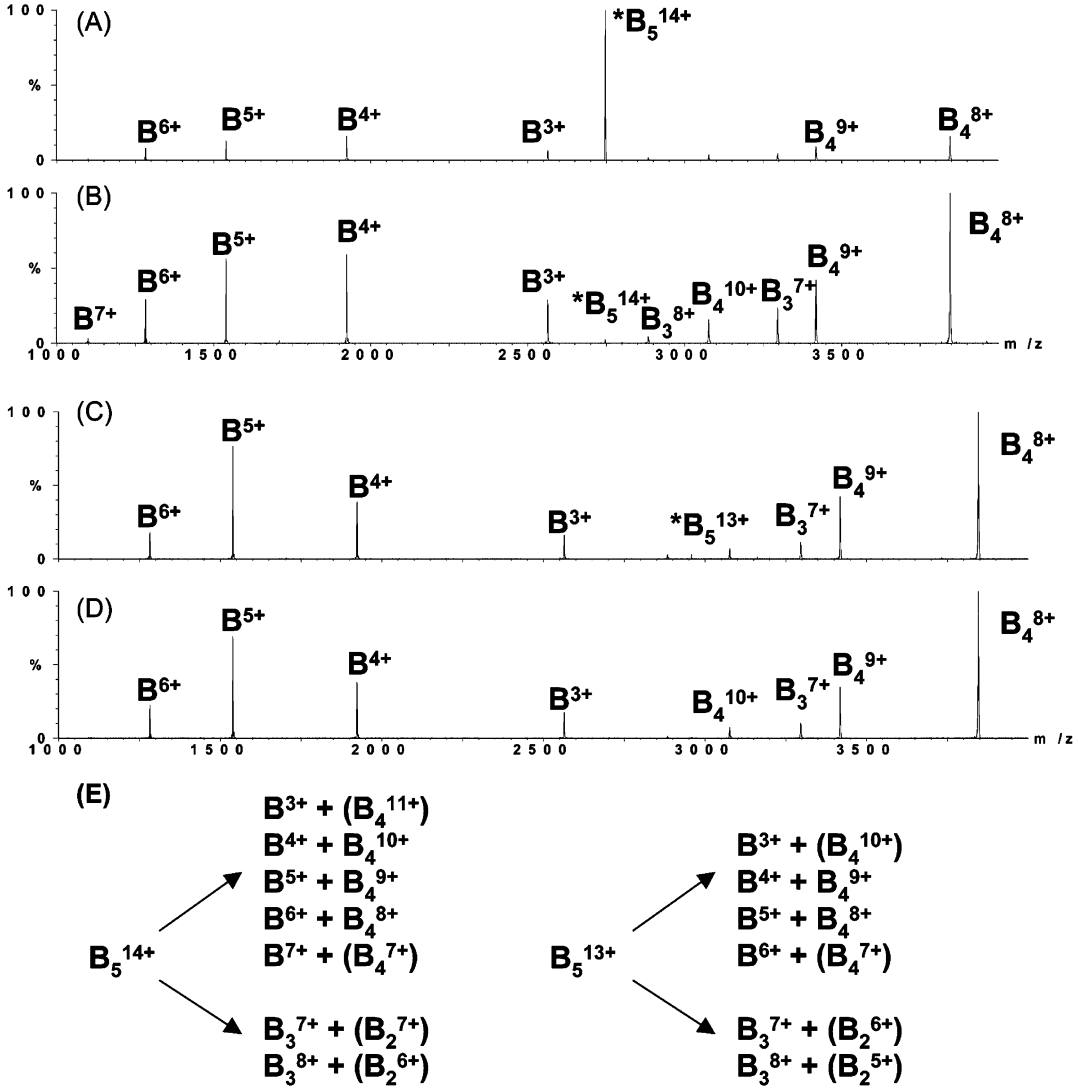

FIGURE 7: ESI triple-quadrupole MS/MS mass spectra of the noncovalent complex of SLT-B_5. Shown is the dissociation obtained at a collision energy of 15 (A) or 25 eV (B) for the precursor B_5^{14+} ion and also the dissociation obtained at a collision energy of 15 (C) or 18 eV (D) for the precursor B_5^{13+} ion. Shown also is the possible dissociation pathway for the B_5^{14+} and B_5^{13+} ions (E).

of individual subunits from the pentamer, tetramer, and trimer ions indicates that the noncovalent interactions maintaining the quaternary structure of the B pentamer are extremely strong. It has been suggested that instability of the complex

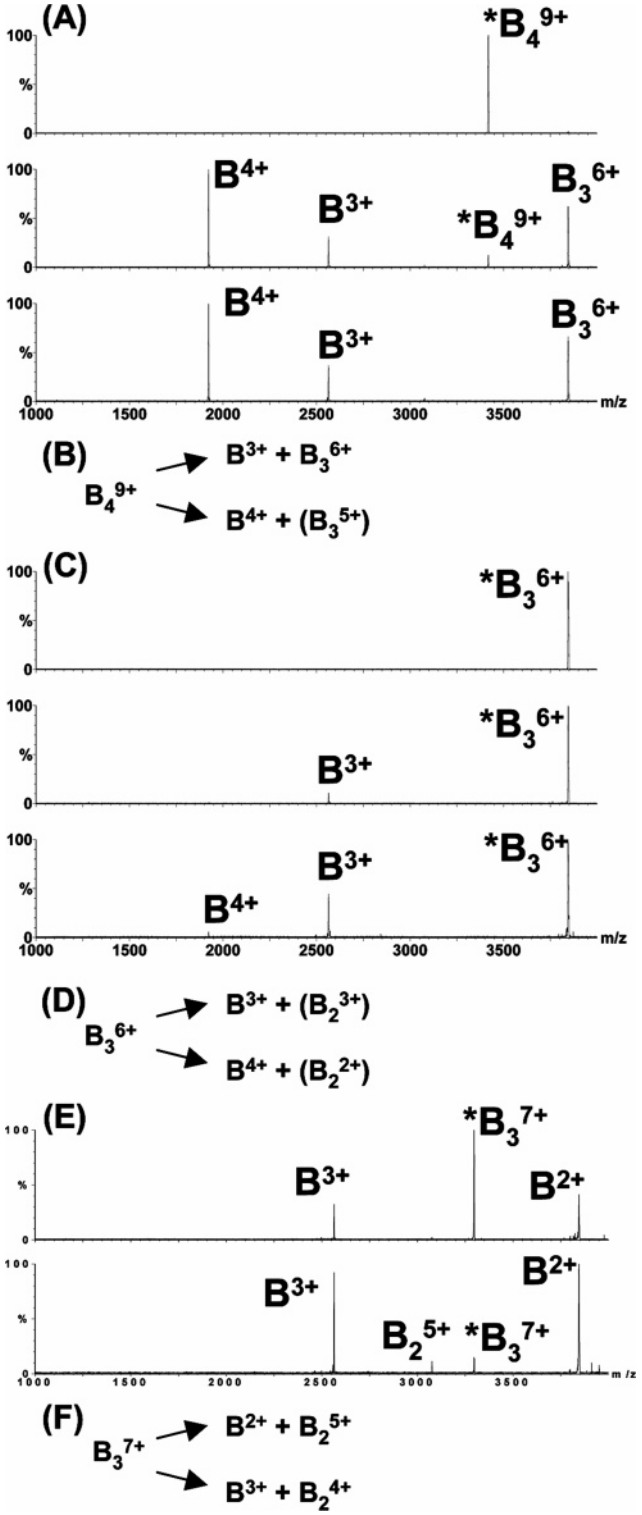

FIGURE 8: ESI triple-quadrupole pseudo-MS/MS/MS mass spectra of the noncovalent complex of SLT-B_5. Shown is the dissociation obtained at a collision energy of 5 eV (no collision gas, top spectrum), 5 eV (with collision gas, middle spectrum), and 15 eV (with collision gas, bottom spectrum) for the precursor B_4^{9+} ion (A) together with the possible dissociation pathway for the B_4^{9+} ion (B). Shown also is the dissociation obtained at a collision energy of 5 eV (no collision gas, top spectrum), 25 eV (with collision gas, middle spectrum), and 40 eV (with collision gas, bottom spectrum) for the precursor B_3^{6+} ion (C) together with the possible dissociation pathway for the B_3^{6+} ion (D). Also shown is the dissociation obtained at a collision energy of 10 eV (with collision gas, top spectrum) and 25 eV (with collision gas, bottom spectrum) for the precursor B_3^{7+} ion (E) together with the possible dissociation pathway for the B_3^{7+} ion (F).

should result upon exposure of the interchain protein surface to solvent, a condition induced in our study by the dissociation of the B_5 parent ion resulting in the loss of a subunit (*49*). However, in the gas phase, intact ions that represented both trimer and tetramer species of the B chain were observed, again indicating the strong nature of the noncovlent interaction in the protein complex. Our findings extend and confirm those of previous reports which suggest that the intersubunit noncovalent interactions of the SLTx B pentamer confer a high degree of stability to the protein complex (*49*, *50*).

CONCLUSIONS

It should be noted that the dissociation of the SLTx complexes is performed in the gas phase, whereas normally the proteins function within an aqueous environment. However, we believe that the data that were obtained are highly relevant, especially due to the near-physiological pH conditions used in this study. Furthermore, clear consistent data were obtained over a range of pH conditions, implying that the noncovalent interactions in the holotoxin are maintained, and observable, under both acidic and neutral conditions. This pH range correlates well with the route of bacterial infection in the host and the striking pH stability of the toxin within the intestinal lumen (*51*, *52*).

In summary, our data for both the SLTx-AB_5 holotoxin and the B_5 pentamer demonstrate that the noncovalent interactions present within this toxin can be rapidly analyzed with the techniques reported here. Since the initial stages of both SLTx-mediated cytotoxicity and cellular signaling are dependent on receptor oligomerization following toxin binding, a rapid technique for examining the oligomeric status of both native and any genetically engineered protein variants will be highly beneficial in further research performed on this toxin.

ACKNOWLEDGMENT

We thank Prof. Robert Freedman and Dr. Catherine Marsden for critical reading of, helpful discussion about, and advice with the manuscript.

REFERENCES

1. O'Brien, A. D., and Holmes, R. K. (1987) Shiga and Shiga-like toxins, *Microbiol. Rev. 51*, 206−220.
2. O'Brien, A. D., Newland, J. W., Miller, S. F., Holmes, R. K., Smith, H. W., and Formal, S. B. (1984) Shiga-like toxin-converting phages from *Escherichia coli* strains that cause hemorrhagic colitis or infantile diarrhea, *Science 226*, 694−696.
3. Marques, L. R., Moore, M. A., Wells, J. G., Wachsmuth, I. K., and O'Brien, A. D. (1986) Production of Shiga-like toxin by *Escherichia coli*, *J. Infect. Dis. 154*, 338−341.
4. Fong, J. S., de Chadarevian, J. P., and Kaplan, B. S. (1982) Hemolytic-uremic syndrome. Current concepts and management, *Pediatr. Clin. North Am. 29*, 835−856.
5. Stein, P. E., Boodhoo, A., Tyrrell, G. J., Brunton, J. L., and Read, R. J. (1992) Crystal structure of the cell-binding B oligomer of verotoxin-1 from *E. coli*, *Nature 355*, 748−750.
6. Fraser, M. E., Chernaia, M. M., Kozlov, Y. V., and James, M. N. (1994) Crystal structure of the holotoxin from Shigella dysenteriae at 2.5 Å resolution, *Nat. Struct. Biol. 1*, 59−64.
7. Richardson, J. M., Evans, P. D., Homans, S. W., and Donohue-Rolfe, A. (1997) Solution structure of the carbohydrate-binding B-subunit homopentamer of verotoxin VT-1 from E. coli, *Nat. Struct. Biol. 4*, 190−193.
8. Endo, Y., Tsurugi, K., Yutsudo, T., Takeda, Y., Ogasawara, T., and Igarashi, K. (1988) Site of action of a Vero toxin (VT2) from

Escherichia coli O157:H7 and of Shiga toxin on eukaryotic ribosomes. RNA N-glycosidase activity of the toxins, *Eur. J. Biochem. 171*, 45−50.
9. Hale, T. L., and Formal, S. B. (1980) Cytotoxicity of Shigella dysenteriae 1 for cultured mammalian cells, *Am. J. Clin. Nutr. 33*, 2485−2490.
10. Waddell, T., Head, S., Petric, M., Cohen, A., and Lingwood, C. (1988) Globotriosyl ceramide is specifically recognized by the *Escherichia coli* verocytotoxin 2, *Biochem. Biophys. Res. Commun. 152*, 674−679.
11. Jacewicz, M., Clausen, H., Nudelman, E., Donohue-Rolfe, A., and Keusch, G. T. (1986) Pathogenesis of shigella diarrhea. XI. Isolation of a shigella toxin-binding glycolipid from rabbit jejunum and HeLa cells and its identification as globotriaosylceramide, *J. Exp. Med. 163*, 1391−1404.
12. Lindberg, A. A., Brown, J. E., Stromberg, N., Westling-Ryd, M., Schultz, J. E., and Karlsson, K. A. (1987) Identification of the carbohydrate receptor for Shiga toxin produced by Shigella dysenteriae type 1, *J. Biol. Chem. 262*, 1779−1785.
13. Garred, O., van Deurs, B., and Sandvig, K. (1995) Furin-induced cleavage and activation of Shiga toxin, *J. Biol. Chem. 270*, 10817−10821.
14. Lea, N., Lord, J. M., and Roberts, L. M. (1999) Proteolytic cleavage of the A subunit is essential for maximal cytotoxicity of *Escherichia coli* O157:H7 Shiga-like toxin-1, *Microbiology 145* (Part 5), 999−1004.
15. Sandvig, K., Garred, O., Prydz, K., Kozlov, J. V., Hansen, S. H., and van Deurs, B. (1992) Retrograde transport of endocytosed Shiga toxin to the endoplasmic reticulum, *Nature 358*, 510−512.
16. Smith, D. C., Lord, J. M., Roberts, L. M., Tartour, E., and Johannes, L. (2002) 1st class ticket to class I: Protein toxins as pathfinders for antigen presentation, *Traffic 3*, 697−704.
17. Sandvig, K., Spilsberg, B., Lauvrak, S. U., Torgersen, M. L., Iversen, T. G., and van Deurs, B. (2004) Pathways followed by protein toxins into cells, *Int. J. Med. Microbiol. 293*, 483−490.
18. Smith, D. C., Lord, J. M., Roberts, L. M., and Johannes, L. (2004) Glycosphingolipids as toxin receptors, *Semin. Cell Dev. Biol. 15*, 397−408.
19. Lee, R. S., Tartour, E., van der Bruggen, P., Vantomme, V., Joyeux, I., Goud, B., Fridman, W. H., and Johannes, L. (1998) Major histocompatibility complex class I presentation of exogenous soluble tumor antigen fused to the B-fragment of Shiga toxin, *Eur. J. Immunol. 28*, 2726−2737.
20. Noakes, K. L., Teisserenc, H. T., Lord, J. M., Dunbar, P. R., Cerundolo, V., and Roberts, L. M. (1999) Exploiting retrograde transport of Shiga-like toxin 1 for the delivery of exogenous antigens into the MHC class I presentation pathway, *FEBS Lett. 453*, 95−99.
21. Haicheur, N., Bismuth, E., Bosset, S., Adotevi, O., Warnier, G., Lacabanne, V., Regnault, A., Desaymard, C., Amigorena, S., Ricciardi-Castagnoli, P., Goud, B., Fridman, W. H., Johannes, L., and Tartour, E. (2000) The B subunit of Shiga toxin fused to a tumor antigen elicits CTL and targets dendritic cells to allow MHC class I-restricted presentation of peptides derived from exogenous antigens, *J. Immunol. 165*, 3301−3308.
22. Haicheur, N., Benchetrit, F., Amessou, M., Leclerc, C., Falguieres, T., Fayolle, C., Bismuth, E., Fridman, W. H., Johannes, L., and Tartour, E. (2003) The B subunit of Shiga toxin coupled to full-size antigenic protein elicits humoral and cell-mediated immune responses associated with a Th1-dominant polarization, *Int. Immunol. 15*, 1161−1171.
23. Ohmura-Hoshino, M., Yamamoto, M., Yuki, Y., Takeda, Y., and Kiyono, H. (2004) Non-toxic Stx derivatives from *Escherichia coli* possess adjuvant activity for mucosal immunity, *Vaccine 22*, 3751−3761.
24. Arab, S., Rutka, J., and Lingwood, C. (1999) Verotoxin induces apoptosis and the complete, rapid, long-term elimination of human astrocytoma xenografts in nude mice, *Oncol. Res. 11*, 33−39.
25. Falguieres, T., Mallard, F., Baron, C., Hanau, D., Lingwood, C., Goud, B., Salamero, J., and Johannes, L. (2001) Targeting of Shiga toxin B-subunit to retrograde transport route in association with detergent-resistant membranes, *Mol. Biol. Cell 12*, 2453−2468.
26. Kovbasnjuk, O., Edidin, M., and Donowitz, M. (2001) Role of lipid rafts in Shiga toxin 1 interaction with the apical surface of Caco-2 cells, *J. Cell Sci. 114*, 4025−4031.
27. Hoey, D. E., Sharp, L., Currie, C., Lingwood, C. A., Gally, D. L., and Smith, D. G. (2003) Verotoxin 1 binding to intestinal crypt epithelial cells results in localization to lysosomes and abrogation of toxicity, *Cell. Microbiol. 5*, 85−97.
28. Thorpe, C. M., Hurley, B. P., Lincicome, L. L., Jacewicz, M. S., Keusch, G. T., and Acheson, D. W. (1999) Shiga toxins stimulate secretion of interleukin-8 from intestinal epithelial cells, *Infect. Immun. 67*, 5985−5993.
29. Gordon, J., Challa, A., Levens, J. M., Gregory, C. D., Williams, J. M., Armitage, R. J., Cook, J. P., Roberts, L. M., and Lord, J. M. (2000) CD40 ligand, Bcl-2, and Bcl-xL spare group I Burkitt lymphoma cells from CD77-directed killing via Verotoxin-1 B chain but fail to protect against the holotoxin, *Cell Death Differ. 7*, 785−794.
30. Tetaud, C., Falguieres, T., Carlier, K., Lecluse, Y., Garibal, J., Coulaud, D., Busson, P., Steffensen, R., Clausen, H., Johannes, L., and Wiels, J. (2003) Two distinct Gb3/CD77 signaling pathways leading to apoptosis are triggered by anti-Gb3/CD77 mAb and verotoxin-1, *J. Biol. Chem. 278*, 45200−45208.
31. Fenn, J. B., Mann, M., Meng, C. K., Wong, S. F., and Whitehouse, C. M. (1989) Electrospray ionization for mass spectrometry of large biomolecules, *Science 246*, 64−71.
32. Krutchinsky, A. N., Chernushevich, I. V., Spicer, V. L., Ens, W., and Standing, K. G. (1998) Collisional Damping Interface for an Electrospray Ionization Time-of-Flight Mass Spectrometer, *J. Am. Soc. Mass Spectrom. 9*, 569−579.
33. Tahallah, N., Pinkse, M., Maier, C. S., and Heck, A. J. (2001) The effect of the source pressure on the abundance of ions of noncovalent protein assemblies in an electrospray ionization orthogonal time-of-flight instrument, *Rapid Commun. Mass Spectrom. 15*, 596−601.
34. Sobott, F., Hernandez, H., McCammon, M. G., Tito, M. A., and Robinson, C. V. (2002) A tandem mass spectrometer for improved transmission and analysis of large macromolecular assemblies, *Anal. Chem. 74*, 1402−1407.
35. Tito, M. A., Tars, K., Valegard, K., Hajdu, J., and Robinson, C. V. (2000) Electrospray Time-of-Flight Mass Spectrometry of the Intact MS2 Virus Capsid, *J. Am. Chem. Soc. 122*, 3550−3551.
36. Fuerstenau, S. D., Benner, W. H., Thomas, J. J., Brugidou, C., Bothner, B., and Siuzdak, G. (2001) Mass Spectrometry of an Intact Virus, *Angew. Chem., Int. Ed. 40*, 541−544.
37. Light-Wahl, K. J., Loo, J. A., Edmonds, C. G., Smith, R. D., Witkowska, H. E., Shackleton, C. H., and Wu, C. S. (1993) Collisionally activated dissociation and tandem mass spectrometry of intact hemoglobin β-chain variant proteins with electrospray ionization, *Biol. Mass Spectrom. 22*, 112−120.
38. Sobott, F., McCammon, M., and Robinson, C. (2003) Gas-phase dissociation pathways of a tetrameric protein complex, *Int. J. Mass Spectrom. 230*, 193−200.
39. Sobott, F., and Robinson, C. (2004) Characterising electrosprayed biomolecules using tandem-MS: The noncovalent GroEL chaperonin assembly, *Int. J. Mass Spectrom. 236*, 25−32.
40. Ferrige, A. G., Seddon, M. J., Green, B. N., Jarvis, S. A., and Skilling, J. (1992) Disentangling electrospray spectra with Maximum Entropy, *Rapid Commun. Mass Spectrom. 6*, 707−711.
41. Miot, M., and Betton, J. M. (2004) Protein quality control in the bacterial periplasm, *Microb. Cell Fact. 3*, 4.
42. Wulfing, C., and Pluckthun, A. (1994) Protein folding in the periplasm of *Escherichia coli*, *Mol. Microbiol. 12*, 685−692.
43. Kitova, E. N., Kitov, P. I., Bundle, D. R., and Klassen, J. S. (2001) The observation of multivalent complexes of Shiga-like toxin with globotriaoside and the determination of their stoichiometry by nanoelectrospray Fourier transform ion cyclotron resonance mass spectrometry, *Glycobiology 11*, 605−611.
44. Saleh, M. T., and Gariepy, J. (1993) Local conformational change in the B-subunit of Shiga-like toxin 1 at endosomal pH, *Biochemistry 32*, 918−922.
45. Jemal, C., Haddad, J. E., Begum, D., and Jackson, M. P. (1995) Analysis of Shiga toxin subunit association by using hybrid A polypeptides and site-specific mutagenesis, *J. Bacteriol. 177*, 3128−3132.
46. Green, B. N., Bordoli, R. S., Hanin, L. G., Lallier, F. H., Toulmond, A., and Vinogradov, S. N. (1999) Electrospray ionization mass spectrometric determination of the molecular mass of the approximately 200-kDa globin dodecamer subassemblies in hexagonal bilayer hemoglobins, *J. Biol. Chem. 274*, 28206−28212.
47. Ling, H., Boodhoo, A., Hazes, B., Cummings, M. D., Armstrong, G. D., Brunton, J. L., and Read, R. J. (1998) Structure of the shiga-like toxin I B-pentamer complexed with an analogue of its receptor Gb3, *Biochemistry 37*, 1777−1788.
48. Hagnerelle, X., Plisson, C., Lambert, O., Marco, S., Rigaud, J. L., Johannes, L., and Levy, D. (2002) Two-dimensional structures

of the Shiga toxin B-subunit and of a chimera bound to the glycolipid receptor Gb3, *J. Struct. Biol. 139*, 113−121.
49. Pina, D. G., Gomez, J., Villar, E., Johannes, L., and Shnyrov, V. L. (2003) Thermodynamic analysis of the structural stability of the shiga toxin B-subunit, *Biochemistry 42*, 9498−9506.
50. Felitsyn, N., Kitova, E. N., and Klassen, J. S. (2001) Thermal decomposition of a gaseous multiprotein complex studied by blackbody infrared radiative dissociation. Investigating the origin of the asymmetric dissociation behavior, *Anal. Chem. 73*, 4647−4661.
51. Karmali, M. A. (2004) Infection by Shiga toxin-producing *Escherichia coli*: An overview, *Mol. Biotechnol. 26*, 117−122.
52. Thorpe, C. M. (2004) Shiga toxin-producing *Escherichia coli* infection, *Clin. Infect. Dis. 38*, 1298−1303.

BI0503706